

Cite this: *Phys. Chem. Chem. Phys.*, 2012, **14**, 6981–6986

www.rsc.org/pccp

PAPER

SnS₂ nanoparticle loaded graphene nanocomposites for superior energy storage

Liwen Ji,^{†a} Huolin L. Xin,^{†b} Teyve R. Kuykendall,^a Shao-Ling Wu,^c Haimei Zheng,^b Mumin Rao,^{cd} Elton J. Cairns,^{cd} Vincent Battaglia^c and Yuegang Zhang^{*a}

Received 13th March 2012, Accepted 14th March 2012

DOI: 10.1039/c2cp40790f

SnS₂ nanoparticle-loaded graphene nanocomposites were synthesized *via* one-step hydrothermal reaction. Their electrochemical performance was evaluated as the anode for rechargeable lithium-ion batteries after thermal treatment in an Ar environment. The electrochemical testing results show a high reversible capacity of more than 800 mA h g⁻¹ at 0.1 C rate and 200 mA h g⁻¹ for up to 5 C rate. The cells also exhibit excellent capacity retention for up to 90 cycles even at a high rate of 2 C. This electrochemical behavior can be attributed to the well-defined morphology and nanostructures of these as-synthesized nanocomposites, which is characterized by high-resolution transmission electron microscopy and electron energy-loss spectroscopy.

Introduction

High-performance rechargeable lithium-ion batteries (LIBs) are indispensable for powering the ever growing needs from advanced electric vehicles (EV), hybrid electric vehicles (HEV) and plug-in hybrid electric vehicles (PHEV). The most popular graphite-based anodes are commonly used in commercially available rechargeable LIBs. However, the graphite can only provide a theoretical specific capacity of about 372 mA h g⁻¹, and therefore it is difficult to meet the increasing demands for various advanced transportation energy storage systems. Hence, it is essential to design and synthesize new anode materials that can offer the promise of high-performance LIBs with elevated efficiency, superior storage capacity, better gravimetric energy density, and longer cycle life.^{1–8}

As a typical layered structure transition metal sulfide, tin disulfide (SnS₂) is suitable for Li ion charge/discharge at high current rates and possesses relatively large theoretical capacity (~645 mA h g⁻¹), because of its unique structural properties, such as large surface area offered by special nanostructures, finite lateral size, and enhanced open-edge morphology.^{9–13} However, bulk or micron sized SnS₂-based anode materials suffer from large volume expansion/contraction and accompanying sharp capacity fading that occurs during prolonged electrochemical

cycling.^{9–13} Downsizing from bulk or micron scale SnS₂ to a variety of nano-morphologies and nanostructures,^{9–13} or dispersing these nanoscaled SnS₂ particles into carbon matrices,^{14,15} is among the most accepted approaches being pursued to overcome these issues and to improve the cycle life and rate capability of SnS₂-based electrodes. The dimension reduction from bulk to nanoscale can help release the huge stresses and strains, accommodate the volume change, and increase the intercalation rate during charging/discharging.^{9–13,16} Adding carbon to SnS₂ can help distribute electrons through the entire electrode, leading to extremely enhanced electrical conductivity.¹⁴ The carbon phase can also act as a buffer layer between electro-active materials and the electrolyte, and minimize electrolyte degradation at the same time.^{3,14,16}

Graphene, a new class of two-dimensional, “aromatic,” monolayer of carbon, has attracted unmatched attention and has also triggered numerous experimental activities, owing to its exceptional properties including high electronic mobility, unique electronic structures, high thermal conductivity and mechanical strength as well as high surface area.^{15,17–20} These unique properties suggest that graphene could be superior to its counterparts (such as graphite, carbon nanotube, *etc.*) as a conductive matrix to enhance electron transport and electrical contact with electrochemically active materials, such as Si, transition metal oxides, transition metal sulfides, *etc.*, in rechargeable LIBs and to effectively prevent their volume expansion/shrinkage and aggregation of these electrochemically active phases during the Li-ion charge/discharge processes.^{15,20–34} Furthermore, its large surface area could also facilitate the absorption of Li atoms on both sides of the sheet or into its ubiquitous cavities and porous structures.³⁵ As a result, graphene-based nanocomposites have excellent electrochemical performance when used as anodes for rechargeable LIBs.^{15,20,23–34}

^a The Molecular Foundry, Lawrence Berkeley National Laboratory, Berkeley, CA 94720, USA. E-mail: yzhang5@lbl.gov

^b Materials Sciences Division, Lawrence Berkeley National Laboratory, Berkeley, CA 94720, USA

^c Environmental Energy Technologies Division, Lawrence Berkeley National Laboratory, Berkeley, CA 94720, USA

^d Department of Chemical & Biomolecular Engineering, University of California, Berkeley, CA 94720, USA

[†] These authors contributed equally to this project.

Herein, SnS₂ nanoparticles, ubiquitously grown on reduced graphene oxide sheets, were synthesized by a simple one-step hydrothermal strategy.³⁶ The electrochemical performance was evaluated as the anode for rechargeable LIBs after thermal treatment in an Ar environment. The electrochemical performance results show a high reversible capacity of more than 800 mA h g⁻¹ at the first cycle at a 0.1 C rate and a reversible capacity of about 200 mA h g⁻¹ even at a high charge/discharge rate of 5 C. Most important of all, these novel nanostructures also show capacity retention for up to 90 cycles even at a high rate of 2 C. This electrochemical behavior can be attributed to the unique morphology and micro-structure of the as-synthesized nanocomposites, and synergistic effects of the different components in the as-prepared nanocomposites.

Experimental

Chemicals

Graphite powder, sodium nitrate (NaNO₃), potassium permanganate (KMnO₄), 96% sulfuric acid (H₂SO₄) solution, 30% hydrogen peroxide (H₂O₂) solution, tin (II) chloride dihydrate (SnCl₂·2H₂O), 36–38% hydrogen chloride (HCl) and thiourea (NH₂CSNH₂) were purchased from Sigma-Aldrich (USA).

Synthesis of the graphite oxides

Graphite oxide was prepared using a modified Hummers method.^{23,37} Firstly, 1 g of natural graphite and 0.875 g of NaNO₃ (purity 99%) were placed in a three-necked flask with a stirrer chip. Then 75 ml of 98% H₂SO₄ was slowly added. The mixture was stirred in an ice-water bath environment for about 2 hours followed by gradually adding 4.5 g of KMnO₄ (purity 99%) over about 2 hours under slow stirring conditions. The as-synthesized mixture was allowed to react for five days at room temperature. Afterwards, 100 ml of 5 wt% H₂SO₄ aqueous solution was added over the course of about 1 h with stirring. The resultant mixture was further stirred for 2 h followed by adding 3 g of 30 wt% H₂O₂ aqueous solution and stirred for another 2 h. This solution was continuously washed thoroughly with a mixed aqueous solution of 3 wt% H₂SO₄/0.5 wt% H₂O₂ many times, and then the purification procedure was similarly repeated three more times using deionized (DI) water (Millipore, 18.2 MΩ cm). The resultant mixture was dispersed in DI water and then centrifuged using an Allegra X-22 centrifuge for 2 hours at 9000 rpm to remove ions of oxidant origins. The remaining dispersion was purified by repeating the same procedure more than 20 times with DI water. Finally, a brown-black homogeneous dispersion was obtained.^{23,37}

Synthesis of the RGO–SnS₂ nanocomposites

The preparation of the RGO–SnS₂ nanocomposite was performed by a one-step hydrothermal approach,³⁶ and the subsequent annealing process at high temperature in an Ar environment.²³ Firstly, 36 mg of graphite oxide was suspended in 36 ml ultrapure water, and sonicated at 50 °C for 5 h to form a stable graphene oxide (GO) dispersion. Then 0.36 ml of hydrochloric acid (HCl, 36–38 wt%) was added, 1 mmol

(225 mg) SnCl₂·2H₂O was also added into the acidic graphene oxide aqueous solution, and the mixture was stirred vigorously for 60 min. After that, 8 mmol (610 mg) NH₂CSNH₂ was added into the mixture and it was stirred vigorously for another 30 min. Finally, the mixture was sealed in a Teflon-lined stainless-steel autoclave of 45 ml capacity. The tank was heated and maintained at 145 °C for 48 h and then cooled to room temperature. The resulting dark reduced graphene oxide–SnS₂ nanocomposite (RGO–SnS₂) was filtered, washed several times using pure ethanol, and dried in a vacuum oven at room temperature followed by further thermal treatment at 400 °C in an Ar environment for 8 hours. In comparison, pure SnS₂ nanoplates with yellow color were also prepared from the same experimental procedures but with no GO.

Materials characterizations

The samples were characterized using scanning electron microscopy (SEM: Zeiss Gemini Ultra-55), energy dispersive X-ray spectrometer (EDX), transition electron microscope (TEM: 200 kV FEI monochromated F20 UT Tecnai equipped with a Gatan imaging filter), thermogravimetric analysis (TGA), and X-ray diffraction (XRD) (Diffraktometer D500/501, Siemens).

Electrochemical measurements

2032 type half cells were assembled with the prepared RGO–SnS₂ nanocomposite as the anode material in a high-purity argon-filled glove box. The RGO–SnS₂ anodes were prepared by mixing RGO–SnS₂ nanocomposites, carbon black, and polyvinylidene difluoride (PVDF) at a weight ratio of 80 : 10 : 10 in NMP solvent to form a slurry. This as-formed slurry was uniformly pasted on pure copper foil and dried at 130 °C for 16 hours. Thin Li foil (0.5 mm thick, FMC lithium) was employed as the counter electrode and a polypropylene membrane (Celgard 2400) was used as the separator. The electrolyte used was 1 M lithium hexafluorophosphate (LiPF₆) dissolved in 1/1 (V/V) ethylene carbonate/ethyl methyl carbonate (EMC) (Ferro Corp.). Cyclic voltammogram (CV) measurements were performed on an AQ4 Gamry Reference 600 electrochemical workstation with a voltage range from 0.001 to 3.0 V at a scan rate of 0.05 mV s⁻¹. Galvanostatic charge (lithium insertion) and discharge (lithium extraction) experiments of the half cells were conducted using an Arbin automatic battery cycler at several different currents between cut-off potentials of 0.001 V and 2.0 V.

Results and discussion

The X-ray diffraction (XRD) pattern of the as-synthesized product in Fig. 1 shows that all the diffraction peaks can be indexed to the SnS₂ phase^{9–11,13,14} along with a very weak 002 peak of carbon, indicating the existence of RGO.^{23–31} While further exploration is necessary, we propose the following mechanism for nanocomposite formation. The functional groups on the surface of GO, such as carboxyl, hydroxyl and epoxy groups, tightly adsorb Sn²⁺ onto the GO surface which is then reduced by NH₂CSNH₂ in the aqueous solution to form RGO.²⁴ At the same time, under acidic conditions, the hydrolysis of NH₂CSNH₂ releases H₂S (S²⁻) at 145 °C, which reacts with

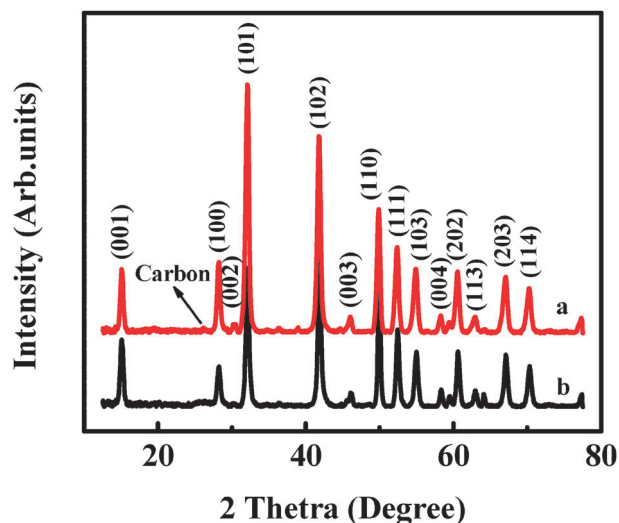


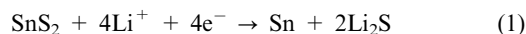
Fig. 1 XRD patterns of the as-synthesized RGO-SnS₂ nanocomposites before (a) and after (b) heat treatment in an Ar environment at 400 °C for 8 hours.

Sn²⁺ to form the SnS₂ nanoparticles. Due to the excess of S²⁻ and H⁺, SnS₂ nuclei were formed in the hydrothermal process. Finally, SnS₂ nanoparticles were grown on the surface of RGO.³⁶

Fig. 2a and b show the SEM images of the as-synthesized RGO-SnS₂ nanocomposite. Large quantities of regular SnS₂ nanoparticles, which have an average size of about 100 nm, are homogeneously dispersed on the wrinkling RGO surface (see SEM image of pure GO and SnS₂ nanoflakes in Fig. S1 and S2, ESI†). The corresponding EDX microanalysis in Fig. 2c confirms the existence of RGO and SnS₂ components in the as-formed nanocomposite. Further insight into the morphology and microstructure of SnS₂ nanoparticles loaded

on RGO is displayed in the TEM image in Fig. 3a. SnS₂ nanoparticles are tightly anchored on the surface or in the cavities/porous structures of the highly conductive graphene sheets. The presence of graphene sheets in the nanocomposites is helpful to stem the aggregation of SnS₂ nanoparticles. The high-resolution transmission electron microscopy (HRTEM) in Fig. 3b shows clear fringes with a separation of 0.58 nm, in good agreement with the interlayer spacing of SnS₂. The corresponding elemental composition mapping of carbon (Fig. 3c), carbon vs. S (Fig. 3d), S (Fig. 3e) and Sn (Fig. 3f) further confirms the blending of carbon and SnS₂ phases on nanometre scale (see Fig. S3–S5 and the detailed analysis, ESI†). Thermal gravimetric analysis shows that our product contains about 82.5 wt% SnS₂ and 17.5 wt% RGO (see Fig. S6 and the analysis, ESI†).

The RGO-SnS₂ nanocomposites were fabricated into anodes for rechargeable LIBs. Fig. 4a shows CV curves of the RGO-SnS₂ nanocomposites measured between 0.001 V and 3.0 V at the scan rate of 0.05 mV s⁻¹. Three broader peaks were present at about 1.8 V, 1.2 V and 0.1 V in the first cathodic potential sweep. The reduction peak at 1.2 V can be assigned to the decomposition of the SnS₂ nanoparticles into metallic Sn and Li₂S (reaction (1)) as well as the formation of solid electrolyte interface (SEI), which may lead to the large irreversibility of SnS₂-based anodes at the first charge/discharge cycle (also see Fig. S7 and the detailed analysis, ESI†).^{9–14,38} This peak is also well consistent with that of the pure SnS₂ as shown in Fig. S8 (ESI†).



The more cathodic potential at around 0.1 V and the anodic potential at about 0.5 V in the first scan are known to represent the redox peak couple of reaction (2). Such a redox

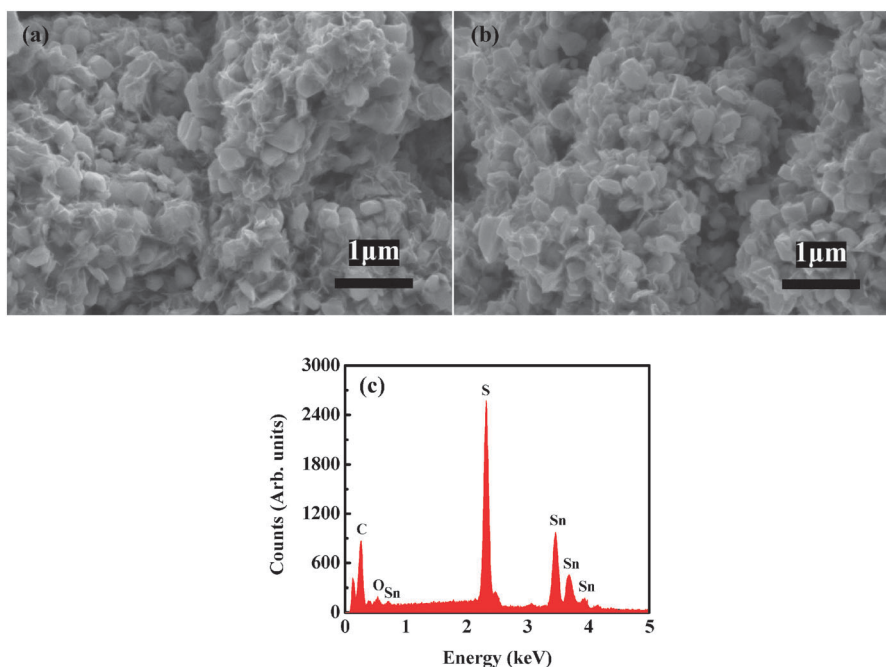


Fig. 2 SEM (a and b) and the corresponding EDX (c) images of the as-synthesized RGO-SnS₂ nanocomposites after heat treatment in an Ar environment at 400 °C for 8 hours.

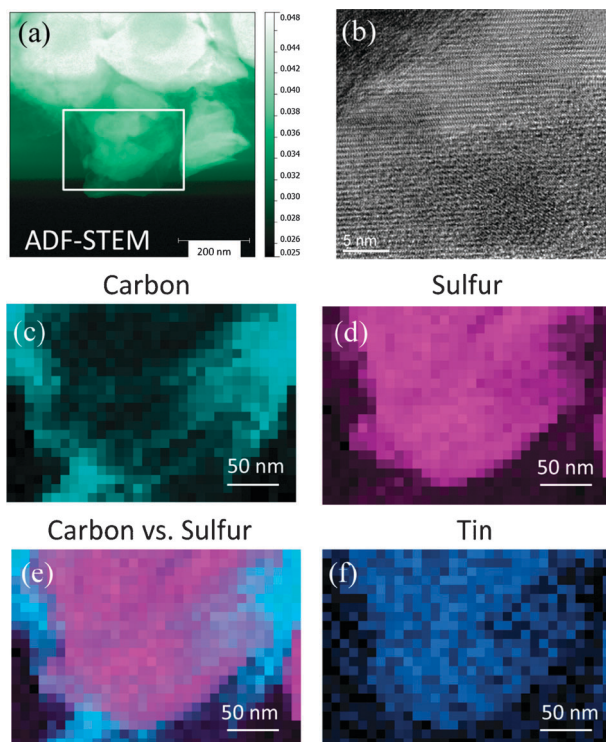
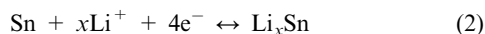
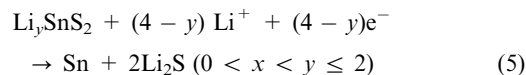
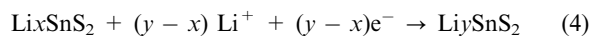
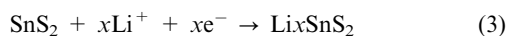


Fig. 3 TEM (a) annular dark-field scanning transmission electron microscopy (ADF-STEM) image and (b) HRTEM image of SnS₂ in the nanocomposite. (c) and (d) show the corresponding STEM electron energy loss spectroscopic mapping of the area indicated by the white frame in (a): (c) carbon (turquoise), (d) sulfur (magenta), (e) sulfur vs. carbon, and (f) tin (blue) maps of the as-synthesized RGO–SnS₂ nanocomposites after heat treatment in an Ar environment at 400 °C for 8 hours.

peak couple was frequently observed in a similar potential range in the following cycles, indicating that Li ions subsequently reacted with Sn metal to form Li_xSn alloy as well as the reverse reaction.^{11,13,14,38,39}



The additional peaks at around 1.6 V and 1.8 V, which were not yet observed during the subsequent cycles, can be attributed to lithium intercalation into the SnS₂ layers without causing phase decomposition, and consequently, reaction (1) may be subdivided into three steps as reactions (3–5).^{10,11,14,38,39} The additional oxidation peaks at around 1.8 V observed in all of the anodic potential scans can be assigned to the lithium deintercalation from SnS₂ layers without phase decomposition. These similar oxidation/reduction peaks are also clearly shown in the CV curve of pure SnS₂ (Fig. S8, ESI†). The CV curve of pure RGO (Fig. S9, ESI†) displays a wide redox peak couple at about 0.5/1.2 V. However, these peaks are absent in RGO–SnS₂. This may be because of the low content of RGO in the nanocomposites. It should be noticed that the electrochemical reaction mechanism between SnS₂ and lithium is complicated during charging/discharging processes, further explorations are still necessary to address this issue.



Galvanostatic charge/discharge testing was also carried out by charging (lithiation) and discharging (delithiation) at different rates in the voltage window of 0.001 V–2.0 V. Fig. 4b shows voltage profiles of the initial ten cycles at 0.1 C (1 C = 645 mA g⁻¹). It was seen that all the charge/discharge curves show plateaus consistent with the peaks in the CV curves and are also well documented in the literature.^{9–14,38} The RGO–SnS₂ electrode clearly exhibits a high discharge capacity of 811 mA h g⁻¹ at the first cycle, with a corresponding coulombic efficiency of about 63.44%, although a large irreversible discharge capacity of about 468 mA h g⁻¹ is obtained at the initial cycle, the coulombic efficiency remains above 98% after this first cycle. This low coulombic efficiency of the prepared RGO–SnS₂ nanocomposite at the first cycle is commonly seen in other reported SnS₂ or C–SnS₂ nanocomposites and should be mainly due to the irreversible reaction (1). The discharge capacity of the second cycle was measured to be 772 mA h g⁻¹, which is still higher than the reported theoretical value for SnS₂. The deviation from the theoretical capacity can be attributed to the special nanostructures which may create some new reaction sites, contributing some extra lithium storage. At the tenth cycle, the reversible capacity remains at about 662 mA h g⁻¹, which is much higher than the capacity of pure SnS₂ and RGO components (see Fig. S8 and S9, ESI†).

This lithium storage capability improvement is further supported by the electrochemical performance comparison between the as-synthesized RGO–SnS₂ nanocomposites and pure SnS₂-based anodes. As shown in Fig. 4c, the capacity remains relatively constant at around 733 mA h g⁻¹ after the initial ten cycles' charging/discharging at a constant current rate of 0.1 C. Although the capacity decreases to about 633 mA h g⁻¹ upon subsequent cycling at a higher current of 0.5 C, the capacity remains at about 405 mA h g⁻¹ after a further 80 cycles at such high rate. In comparison, the as-synthesized pure SnS₂ can deliver a first cycle discharge capacity of about 584 mA h g⁻¹, which decreases to 215 mA h g⁻¹ after the 10th cycle (see charge/discharge profiles in Fig. S8b, ESI†). This capacity is 78 mA h g⁻¹ at the first cycle upon further cycling at 0.5 C. Further cycling leads to a total capacity loss after 10 cycles (Fig. 4c). Enormous volume expansion and contraction during the continuous alloying/dealloying reactions and the absence of graphene buffer layers may damage the structural integrity of pure SnS₂-based anodes, leading to loss of electrical contact, and resulting in poor capacity retention.^{9–11,13,14,38} We also believe that the build-up of insulating Li₂S may also contribute to the capacity decay (see Fig S7 and the detailed analysis there, and also see the CV curve of synthesized SnS₂ in Fig. S8a, ESI†). The pure RGO anodes deliver a relatively small initial discharge capacity of about 335 mA h g⁻¹ at 0.1 C, although this capacity shows a slight fading in the subsequent cycling, the capacity remains constant at the following rate of 0.5 C (Fig. S9b and c, ESI†). We attribute the significantly enhanced performance of the as-synthesized RGO–SnS₂ nanocomposites to the unique structures and the synergistic effects of different components. On the one hand,

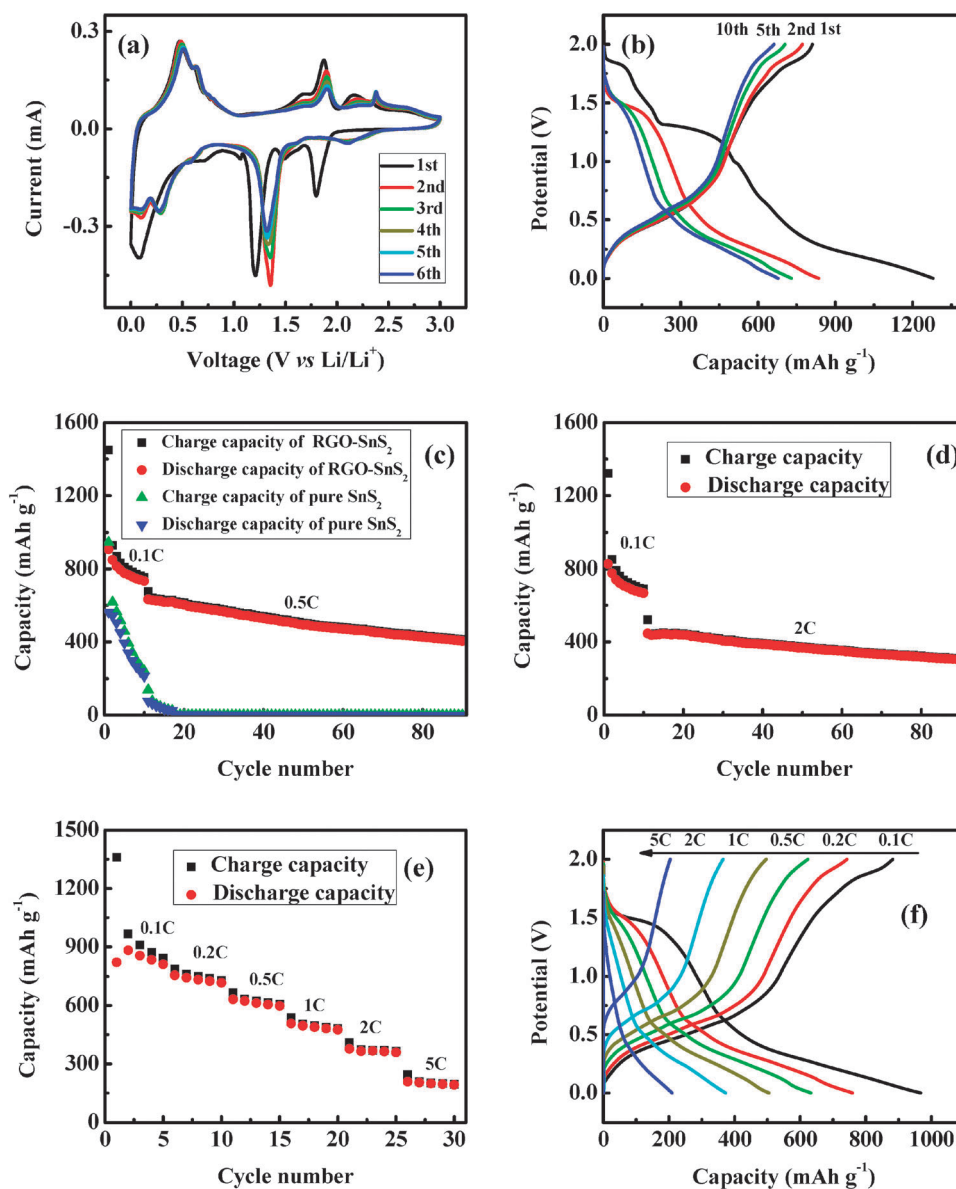


Fig. 4 (a) CV curve of RGO-SnS₂ nanocomposites at 0.05 mV s⁻¹ scanning rate in the potential window from 0.001 V to 3.0 V (vs. Li⁺/Li); (b) galvanostatic charge/discharge profiles of RGO-SnS₂ nanocomposites at a cycling rate of 0.1 C; cycling performance of the RGO-SnS₂ nanocomposites at rates of 0.5 C (c), and 2 C (d), respectively; (e and f) reversible capacity vs. current density (rate capability) for RGO-SnS₂ nanocomposites. All the coin cells were cycled in the potential window from 0.001 V to 2.0 V.

the novel structures enable the intimate interaction between RGO and SnS₂ nanoparticles grown on them which can lead to greater accessibility to the electrolyte, facilitate the diffusion and transfer of Li-ions and electrons between them.^{24,40} At the same time, the reliable mechanical and electrical contact can buffer local volume changes and maintain the integrity of the electrodes during cycling. On the other hand, the novel structures can merge the virtues of both graphene and SnS₂ nanoparticle phases and offer more electrochemically active sites for the reversible accommodation of lithium. The unique nanocomposites may also increase the reversibility of the reaction (1) similar to the GO-S cathode material.⁴¹ These combined factors make the as-synthesized RGO-SnS₂ nanocomposite anodes exhibit larger reversible capacity and enhanced cycle performance.

Further cycling tests at higher currents also show that the RGO-SnS₂ nanocomposite anodes exhibit excellent cycle life and rate capability even at higher current rates. Fig. 4d shows cycling of another RGO-SnS₂ nanocomposite anode at a high current of 2 C after the initial ten cycles at 0.1 C. The capacity at the 2 C rate is about 446 mA h g⁻¹ in the first cycle and remains at about 304 mA h g⁻¹ after 80 cycles, indicating a relatively slow capacity fading, which also plagues pure SnS₂-based anodes (Fig. S8c, ESI†). Another example of the high-rate capability of the RGO-SnS₂ nanocomposite anode is demonstrated in Fig. 4e where a half cell retains stable capacity of about 500 mA h g⁻¹ at 1 C, about 400 mA h g⁻¹ at about 2 C, and a capacity of 200 mA h g⁻¹ still can be obtained at a high rate of 5 C after 30 cycles of changeable current rates (also see the corresponding charge/discharge

profiles in Fig. 4f). To our knowledge, there are still few reports that evaluate the electrochemical behavior of C/SnS₂ nanocomposite-based electrodes at such high rates.¹⁴ These results further demonstrate that the rationally synthesized RGO–SnS₂ nanocomposites can combine the excellent electronic conductivity of graphene and the high electrochemical capacity of SnS₂ to achieve improved cycle performance and rate capability in rechargeable LIBs. The excellent electrical conductivity of graphene ensures good electrical contact with the adjacent SnS₂ nanoparticles. These features would also facilitate the diffusion of Li-ion and electron transfer within the host matrix during charge and discharge, shorten the diffusion distance of Li-ions and significantly enhance the lithium insertion–extraction kinetics.

In summary, we synthesized RGO–SnS₂ nanocomposites by a simple hydrothermal approach. The as-synthesized nanocomposites with unique structures can deliver a highly reversible capacity of about 800 mA h g⁻¹ when used as an anode in rechargeable LIBs and the excellent capacity retention of about 64%, and 68% after 90 cycles at rates of 0.5 C and 2 C, respectively, which is much better than pure SnS₂-based anodes. The improved performance may be attributed to the well-defined nanostructures which lead to maximum utilization of the unique properties of both electrochemically active SnS₂ nanoparticles and graphene sheets together in LIBs with high reversible capacity and excellent discharge rates.

Acknowledgements

This work was supported by the Office of Science, Office of Basic Energy Sciences, of the U. S. Department of Energy under contract No. DE-AC02-05CH11231. HLX thanks Qingyun Mao of Cornell University for the FEFF simulations of the sulfur L_{2,3} edges.

Notes and references

- 1 M. Armand and J. M. Tarascon, *Nature*, 2008, **451**, 652–657.
- 2 K. T. Lee and J. Cho, *Nano Today*, 2011, **6**, 28–41.
- 3 L. Ji, Z. Lin, M. Alcoutlabi and X. Zhang, *Energy Environ. Sci.*, 2011, **4**, 2682–2699.
- 4 C. Liu, F. Li, L.-P. Ma and H.-M. Cheng, *Adv. Mater.*, 2010, **22**, E28–E62.
- 5 Y.-G. Guo, J.-S. Hu and L.-J. Wan, *Adv. Mater.*, 2008, **20**, 2878–2887.
- 6 L. Q. Mai, B. Hu, W. Chen, Y. Y. Qi, C. S. Lao, R. S. Yang, Y. Dai and Z. L. Wang, *Adv. Mater.*, 2007, **19**, 3712–3716.
- 7 B. Scrosati, J. Hassoun and Y.-K. Sun, *Energy Environ. Sci.*, 2011, **4**, 3287–3295.
- 8 X. Zhang, L. Ji, O. Toprakci, Y. Liang and M. Alcoutlabi, *Polym. Rev.*, 2011, **51**, 239–264.
- 9 J.-W. Seo, J.-T. Jang, S.-W. Park, C. Kim, B. Park and J. Cheon, *Adv. Mater.*, 2008, **20**, 4269–4273.
- 10 C. Zhai, N. Du, H. Zhang and D. Yang, *Chem. Commun.*, 2011, **47**, 1270–1272.
- 11 T.-J. Kim, C. Kim, D. Son, M. Choi and B. Park, *J. Power Sources*, 2007, **167**, 529–535.
- 12 H. Mukaibō, A. Yoshizawa, T. Momma and T. Osaka, *J. Power Sources*, 2003, **119–121**, 60–63.
- 13 T. Momma, N. Shiraiishi, A. Yoshizawa, T. Osaka, A. Gedanken, J. Zhu and L. Sominski, *J. Power Sources*, 2001, **97–98**, 198–200.
- 14 H. S. Kim, Y. H. Chung, S. H. Kang and Y.-E. Sung, *Electrochim. Acta*, 2009, **54**, 3606–3610.
- 15 B. Luo, Y. Fang, B. Wang, J. Zhou, H. Song and L. Zhi, *Energy Environ. Sci.*, 2012, **5**, 5226–5230.
- 16 J. M. Tarascon, *Philos. Trans. R. Soc. London, Ser. A*, 2010, **368**, 3227–3241.
- 17 Y. Zhu, S. Murali, W. Cai, X. Li, J. W. Suk, J. R. Potts and R. S. Ruoff, *Adv. Mater.*, 2010, **22**, 3906–3924.
- 18 K. Evanoff, A. Magasinski, J. Yang and G. Yushin, *Adv. Energy Mater.*, 2011, **1**, 495–498.
- 19 C. X. Guo, M. Wang, T. Chen, X. W. Lou and C. M. Li, *Adv. Energy Mater.*, 2011, **1**, 736–741.
- 20 Y. Sun, Q. Wu and G. Shi, *Energy Environ. Sci.*, 2011, **4**, 1113–1132.
- 21 J. Liu, G. Cao, Z. Yang, D. Wang, D. Dubois, X. Zhou, G. L. Graff, L. R. Pederson and J.-G. Zhang, *ChemSusChem*, 2008, **1**, 676–697.
- 22 Z.-S. Wu, W. Ren, L. Wen, L. Gao, J. Zhao, Z. Chen, G. Zhou, F. Li and H.-M. Cheng, *ACS Nano*, 2010, **4**, 3187–3194.
- 23 L. Ji, Z. Tan, T. R. Kuykendall, S. Aloni, S. Xun, E. Lin, V. Battaglia and Y. Zhang, *Phys. Chem. Chem. Phys.*, 2011, **13**, 7170–7177.
- 24 K. Chang and W. Chen, *Chem. Commun.*, 2011, **47**, 4252–4254.
- 25 L. Ji, Z. Tan, T. R. Kuykendall, E. J. An, Y. Fu, V. Battaglia and Y. Zhang, *Energy Environ. Sci.*, 2011, **4**, 3611–3616.
- 26 B. Li, H. Cao, J. Shao, H. Zheng, Y. Lu, J. Yin and M. Qu, *Chem. Commun.*, 2011, **47**, 3159–3161.
- 27 J. Choi, J. Jin, I. G. Jung, J. M. Kim, H. J. Kim and S. U. Son, *Chem. Commun.*, 2011, **47**, 5241–5243.
- 28 B. Wang, X.-L. Wu, C.-Y. Shu, Y.-G. Guo and C.-R. Wang, *J. Mater. Chem.*, 2010, **20**, 10661–10664.
- 29 Y. Zou and Y. Wang, *Nanoscale*, 2011, **3**, 2615–2620.
- 30 J. S. Chen, Z. Wang, X. C. Dong, P. Chen and X. W. Lou, *Nanoscale*, 2011, **3**, 2158–2161.
- 31 J. Xiao, X. Wang, X.-Q. Yang, S. Xun, G. Liu, P. K. Koech, J. Liu and J. P. Lemmon, *Adv. Funct. Mater.*, 2011, **21**, 2840–2846.
- 32 J. Zhu, T. Zhu, X. Zhou, Y. Zhang, X. W. Lou, X. Chen, H. Zhang, H. H. Hng and Q. Yan, *Nanoscale*, 2011, **3**, 1084–1089.
- 33 L. Ji, H. Zheng, A. Ismach, Z. Tan, S. Xun, E. Lin, V. Battaglia, V. Srinivasan and Y. Zhang, *Nano Energy*, 2012, **1**, 164–171.
- 34 D. Wang, D. Choi, J. Li, Z. Yang, Z. Nie, R. Kou, D. Hu, C. Wang, L. V. Saraf, J. Zhang, I. A. Aksay and J. Liu, *ACS Nano*, 2009, **3**, 907–914.
- 35 D. Pan, S. Wang, B. Zhao, M. Wu, H. Zhang, Y. Wang and Z. Jiao, *Chem. Mater.*, 2009, **21**, 3136–3142.
- 36 J. Feng, J. Chen, B. Geng, H. Feng, H. Li, D. Yan, R. Zhuo, S. Cheng, Z. Wu and P. Yan, *Appl. Phys. A: Mater. Sci. Process.*, 2010, **103**, 413–419.
- 37 M. Hirata, T. Gotou, S. Horiuchi, M. Fujiwara and M. Ohba, *Carbon*, 2004, **42**, 2929–2937.
- 38 S. Liu, X. Yin, L. Chen, Q. Li and T. Wang, *Solid State Sci.*, 2010, **12**, 712–718.
- 39 J. Zai, K. Wang, Y. Su, X. Qian and J. Chen, *J. Power Sources*, 2011, **196**, 3650–3654.
- 40 H. Hwang, H. Kim and J. Cho, *Nano Lett.*, 2011, **11**, 4826–4830.
- 41 L. Ji, M. Rao, H. Zheng, L. Zhang, Y. Li, W. Duan, J. Guo, E. J. Cairns and Y. Zhang, *J. Am. Chem. Soc.*, 2011, **133**, 18522–18525.